

Controlling submicron-particle template morphology: effect of solvent chemistry

Maria M. Cortalezzi^a, Vicki Colvin^a, Mark R. Wiesner^{a,*}

^a *Energy and Environmental Systems Institute, Rice University, Houston, TX, USA*

^b *Department of Chemistry, Rice University, Houston, TX, USA*

Received 14 July 2003; accepted 26 August 2004

Abstract

Porous solids were obtained from self-assembled deposits of silica particles used as templates to form 3-D porous membranes. The effect of the solvent chemistry on the morphology of the deposits was investigated. The parameters of interest are surface tension and ionic strength of the solvent, as they impact electrostatic and capillary interactions. Deposits of particles of different sizes were obtained from a variety of conditions. The deposits were imaged by SEM and showed distinctive structures for each of the solvent chemistries. The phenomenon is qualitatively consistent with DLVO theory and calculations of capillary interaction energy as developed by Kralchevsky and co-workers.

© 2004 Elsevier Inc. All rights reserved.

1. Introduction

There is general consensus that the utility of a porous material depends on the internal pore diameter, the pore size distribution, and the morphology [1]. Traditional methods for the fabrication of porous materials such as stretching, track-etching, or phase inversion can produce membranes with one-dimensional channel structures and have relatively little control over the pore size distribution [2]. The unavailability of methods for producing materials with uniform sub-micrometer pores [3] and, more specifically, a gap in preparation methods of porous materials in the 10–100 nm range [4] have been recognized.

Porous solids can be created from colloidal crystal templates, or more generally, from deposits of particles on substrates. The voids in the deposits can be filled with a polymeric or inorganic material, and upon removal of the particles a porous material with a three-dimensional structure is formed.

Current fabrication methods lack the ability to precisely control the pore size and pore morphology and are restricted

to specific materials. The template-derived process provides the means to fabricate three-dimensional porous membranes that have well-defined and well-controlled pore sizes, completely interconnected pores and highly ordered structures. The morphology of the pore structure may be tailored at the nanoscale. Recent interest in the template-derived porous materials arises in part from the variety of materials, pore sizes and pore structures potentially accessible through this procedure. The method has been described as powerful, inexpensive and controllable, holding promise for the formation of advanced new materials [5].

The deposition of colloidal particles may occur by different mechanisms: gravity sedimentation from dispersions, filtration, centrifugal sedimentation, sedimentation in capillaries, colloidal solutions spun coated onto surfaces, or capillary forces. The problems in gravity sedimentation are that it gives rise to polycrystalline domains of unknown sizes, the formation of crystals occurs only at specific volume fractions of the colloids, and the growth and thickness are difficult to adjust and control. Several researchers have reported the preparation of porous materials by filtration of a particle suspension in a packing cell [2–4]. The method resulted in regions of order separated by grain boundaries [4]. In the case of ceramics, the membranes were too fragile to withstand

* Corresponding author. Fax: +1-713-348-5203.

E-mail address: wiesner@rice.edu (M.R. Wiesner).

pressure during filtration [2]. The self-assembly technique by capillary forces provides precise control of the thickness of the film through sphere size and concentration in solution [6].

Previous work has shown that particle size, particle concentration, meniscus height, solvent evaporation rate, and shape of liquid surface have an important effect on colloidal crystal growth. Particle size and concentration, and meniscus height are related to the final multilayer thickness when grown in a stationary substrate; evaporation rate has some effect on the film uniformity but not on the thickness [6].

The morphology of particle deposits appears to be a function of the depositional trajectory, particle surface chemistry, and the history of deposit reorganization [7]. The role of depositional trajectory has been demonstrated in earlier work [8]. Kim and Rajagopalan (1991) presented simulation results on the effect of particle surface chemistry on deposit morphology. In this paper, we investigate the effect of the surface tension and ionic strength of the solvent on the morphology of the particle deposits, as a tool to obtain the desired pore structures in fabricating membrane template from particles.

2. Theory

Denkov et al. [9] proposed that an attractive capillary force was the driving force for the mechanism of colloidal crystal formation on a horizontal substrate. This force is directly proportional to the surface tension of the suspension, as well as to other parameters such as the difference in densities between liquid and gas, distance between particles and meniscus slope angle. In a later work, Dimitrov et al. [10] proposed a relationship between the rate of colloidal crystal growth on a vertical substrate, its withdrawal rate from the suspension, and the number of layers formed. Jiang et al. [6] modified this equation for the case of a stationary substrate and expressed the layers of particles formed as a function of the particle diameter, particle concentration, and meniscus height by

$$N_L = \frac{\beta L \varphi}{0.605d(1 - \varphi)}, \quad (1)$$

where N_L is the final number of layers, β is a coefficient that depends on particle–particle and particle–substrate interactions and varies from 0 to 1 (for dilute suspensions of nonadsorbing particles it can be taken as 1), φ is the particle volume fraction, d is the particle diameter, and L is the meniscus height.

The energy of interaction and the resulting forces between the particles are theorized to produce deposits with different morphologies. The principles of particle interactions through electrostatic and capillary forces are briefly reviewed as a basis for interpreting experimental results.

2.1. DLVO forces

DLVO theory describes the potential energy of particle interaction as a function of interparticle distance due to electrostatic and van der Waals forces [11].

The repulsion potential is given by

$$\Phi_R = \frac{64\pi R n_0 k T \gamma_0^2}{\kappa} \exp(-\kappa s), \quad (2)$$

where R is the radius of the particle, n_0 the bulk ionic concentration, k the Boltzmann constant, T the temperature, κ the inverse Debye length, s the interparticle distance, and γ_0 is given by the following expression:

$$\gamma_0 = \frac{\exp(z e \psi_0 / 2kT) - 1}{\exp(z e \psi_0 / 2kT) + 1}, \quad (3)$$

where z is the valence of the ions in solution, e is the charge of the electron, and ψ_0 is the potential at the surface that can be obtained from electrophoretic measurements.

The inverse Debye length is given by

$$\kappa = \left(\frac{8\pi e^2 N_A I}{1000 \epsilon k T} \right)^{0.5}, \quad (4)$$

where N_A is the Avogadro number, I is the ionic strength of the solvent, and ϵ is the relative dielectric permittivity of the solvent.

For low potentials, the following simplified expression can be used:

$$\Phi_R = \frac{1}{2} \epsilon R \psi_0^2 \exp(-\kappa s). \quad (5)$$

The attraction potential due to van der Waals forces can be calculated by the following equation [12]:

$$\Phi_A = \frac{-A}{6} \left[\frac{2R^2}{s + 4Rs} + \frac{2R^2}{s^2 + 4Rs + 4R^2} + \ln \left(\frac{s^2 + 4Rs}{s^2 + 4Rs + 4R^2} \right) \right], \quad (6)$$

where A is the Hamaker constant that depends both on the solvent and on the particles, R is the radius of the particle, and s is the interparticle distance.

The repulsion forces decay exponentially with distance. The exponential coefficient, the inverse Debye length, monotonically increases with the ionic strength of the medium. Thus, an increase in the ionic strength of the solvent will lower the range of the repulsion forces by increasing the coefficient in the exponential but will have no effect in the attraction potential. The increase in ionic strength will also cause a decrease in the zeta potential, and thus the Stern potential of the particles. The net force affecting the particles will change, favoring the attraction forces and facilitating aggregation.

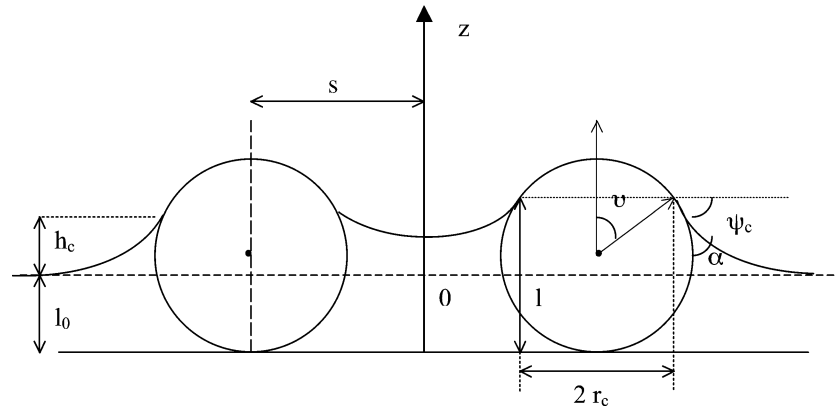


Fig. 1. Schematic description of the problem: a flat plate covered with a liquid layer of thickness l_0 , from which two particles of diameter $2R > l_0$ protrude.

2.2. Capillary forces

The deformation of a liquid–fluid interface due to trapped colloidal particles gives rise to capillary forces exerted on the particles. These forces are usually attractive and lead to the formation of clusters. Kralchevsky et al. [13] developed a set of equations to calculate the capillary interaction energy between colloidal particles partially immersed in a liquid, by solving the Laplace equation for the interface. Fig. 1 depicts the situation considered: a flat plate covered with a liquid layer of thickness l_0 , from which two particles of diameter $2R > l_0$ protrude.

The solution assumes a small inclination of the contact line from the horizontal position, in which case the horizontal projection of the contact line can be approximated by a circumference of radius r_c and a small slope of the meniscus surface; the condition is always satisfied with small floating number (small Bond number) [14].

The interaction energy ΔW between the particles due to capillary forces can be calculated by

$$\Delta W(s) = -2\pi\gamma [2(h_c - h_\infty)R \cos \alpha - r_c h_c \sin \Psi_c + r_c^2 + r_\infty h_\infty \sin \Psi_\infty - r_\infty^2] - 2\Delta\rho g \left(\int_{V1} z dV - \int_{V1\infty} z dV \right). \tag{7}$$

By means of the Green theorem, the integrals over the meniscus volume and surface in the second term in Eq. (7) are transformed to integrals over the 3-phase contact line, leading to

$$\int_{V1} z dV - \int_{V1\infty} z dV = \frac{\pi}{2} \left\{ \frac{1}{2}(h_c^2 - h_\infty^2)[2l_0(2R - l_0) - h_c^2 - h_\infty^2] + \frac{4}{3}(R - l_0)(h_c^3 - h_\infty^3) - r_c^2 h_c^2 + r_\infty^2 h_\infty^2 \right\}. \tag{8}$$

This value usually turns out to be negligible as shown by the numerical calculations [13].

The two sets of equations to be solved are:

$$r_\infty = \sqrt{l_\infty(2R - l_\infty)}, \tag{9}$$

$$\Psi_\infty = \arcsin\left(\frac{r_\infty}{R}\right) - \alpha, \tag{10}$$

$$l_\infty = l_0 - r_\infty \sin \Psi_\infty \ln\left(\frac{\gamma_e q r_\infty (1 + \cos \Psi_\infty)}{4}\right), \tag{11}$$

where $\ln \gamma_e$ is the Euler–Masceroni number ($\gamma_e = 1.781072418$),

$$q = \sqrt{\frac{\Delta\rho g}{\gamma}}, \tag{12}$$

$$h_\infty = r_\infty \sin \Psi_\infty \ln\left(\frac{2}{\gamma_e q r_\infty}\right), \tag{13}$$

and at each interparticle distance s :

$$r_c = \sqrt{l(2R - l)}, \tag{14}$$

$$a = \sqrt{s^2 - \frac{r_c^2}{l}}, \tag{15}$$

$$\Psi_c = \arcsin\left(\frac{r_c}{R}\right) - \alpha, \tag{16}$$

$$\tau_1 = \ln\left(\frac{a}{r_c} + \sqrt{1 + \frac{a^2}{r_c^2}}\right). \tag{17}$$

The variables that have effects on these forces are the density difference between the liquid and the air, the liquid surface tension, and thickness of the liquid film in which the particles are immersed.

3. Experimental

Silica particles of sizes ranging between 100 and 300 nm were used. Silica particles of two sources were used: some were prepared in the laboratory following the Stöber–Fink–Bohn method [15], and the others were obtained from Nissan Chemical Industries, Ltd. The particle average size, standard deviation of their size distribution and sources are shown

Table 1
Size distribution and sources of the silica particles

Particle type	Mean particle size (nm) ^a	Standard deviation	Source ^b
Si 300	305	9%	(1)
Si 250	244	7%	(1)
PST 1	88	21%	(2)

^a Particle size distribution measured by scanning electron microscopy.

^b Silica particles of two sources were used: (1) prepared in the laboratory following the Stöber–Fink–Bohn method [15], (2) from Nissan Chemical Industries, Ltd.

Table 2
Solvent characteristics used in the deposition experiments: ethanol, ultrapure water, and four aqueous solutions of CaCl₂ of different ionic strength

Solvent	[CaCl ₂] (m/l)	Ionic strength (M)	γ (mN/m, 20 °C) [16]
Ethanol	0	–	22.800
Water	0	–	72.750
1-IS	0.0004	0.0012	72.752
2-IS	0.04	0.12	72.911
3-IS	0.05	0.15	72.951
4-IS	0.5	1.5	74.760

in Table 1. Zeta potentials were determined by MALVERN Zeta Meter.

Suspensions of the particles in different solvents were prepared. Each one was washed at least three times to ensure there was no contamination from the solvent in which the particles were initially obtained. CaCl₂ (Aldrich, Milwaukee, WI) was added to the aqueous suspensions to increase ionic strength. The surface tension of CaCl₂ solutions was calculated using the correlations given by Weissenborn et al. [16], who studied the surface tension of high ionic strength aqueous solutions. The solvents used in this study and their characteristics are presented in Table 2.

Glass microslides were carefully cleaned with ethanol and then placed vertically into glass vials containing approximately 10 ml of a particle suspension. Upon evaporation of the liquid, the silica particles deposited on the microslide. The deposits were imaged by SEM using a Philips XL 30 ESEM. Previous to imaging, the samples were coated with gold using a CrC 100 sputtering system (Plasma Sciences, Inc.) to create a conductive surface.

4. Results and discussion

The deposits were imaged with SEM in order to observe the resulting morphologies. In all cases, the ethanol and pure water suspensions gave deposits with a uniform arrangement of particles resembling the hexagonal packing of spheres. The deposits formed from ethanol have slightly more ordered structures; this can be attributed to the difference of surface tension of the solvents; the decrease of surface tension in the case of ethanol facilitates the meniscus deformation and increases the magnitude of the capil-

lary interaction [17]. The attractive capillary forces between the particles are thus stronger and result in a more compact arrangement. This effect was not so clearly observed for the PST1 particles. These particles have a higher standard deviation of the size distribution that negatively affects the packing regularity during deposition. As the ionic strength of the solvent increases, the structure of the deposits tends to be more open and for the higher ionic strength cases the structures exhibited tree-like morphologies, with branches composed of clusters of particles that grew from the relatively more compact arrangement of the first layers.

The deposition process can be conceptually divided into two steps. First, the particles in the suspension approach the glass slide as the liquid evaporates, and they attach. The second step is the drying of the liquid film that partially covers the deposited particles. In this step, the capillary forces attract the particles closer together and thus an ordered and compact structure is formed. In the case of ethanol, for example, the particles are subjected to a net repulsive force while in suspension and they approach the glass slide individually to form the deposit. However, when the particles are suspended in a high-ionic-strength solvent, the potential barrier that prevented the particles from attaching in the previous case is much lower and can be overcome. Thus, aggregates are formed in the bulk of the suspension before deposition, and the particles do not approach the glass slide one by one but rather in aggregates. As a result, open, tree-like structures are formed. The higher the ionic strength, the less the repulsive interactions between the particles become, and more particles deposit as aggregates with a more disorganized structure.

The ability to obtain deposits with variable morphology provides a way to design the pore structure of template-derived membranes. Five to ten layers of small spheres constitute an optimal template for the active filtration layer of an asymmetric membrane, while an open deposit of bigger particles will form a good membrane support, giving mechanical strength without compromising hydraulic permeability.

Fig. 2 shows the SEM images corresponding to deposits of silica particles with an average diameter of 244 nm. Case (a) is a deposit from ethanol, (b) from an aqueous solution of 0.15 M ionic strength, and (c) from an aqueous solution of 1.5 M ionic strength. In the case of ethanol, the particles experience a net repulsive force in the bulk and they approach the glass surface individually to form the deposit. When the particles are suspended in the high ionic strength solvent (cases (b) and (c)), aggregates are formed in the bulk and the deposition process is one of clusters in lieu of individual particles. The higher the ionic strength of the solvent, the more open the deposit morphology. Similar trends were observed in template formation using 88 nm silica particles (Fig. 3). Deposits from suspensions in ultrapure water (a) were similar to those formed at from suspensions in a low ionic strength (0.001 M) solution (b). The relatively broad particle size distribution of these smaller particles tends to obscure any differences that may occur between these two solutions.

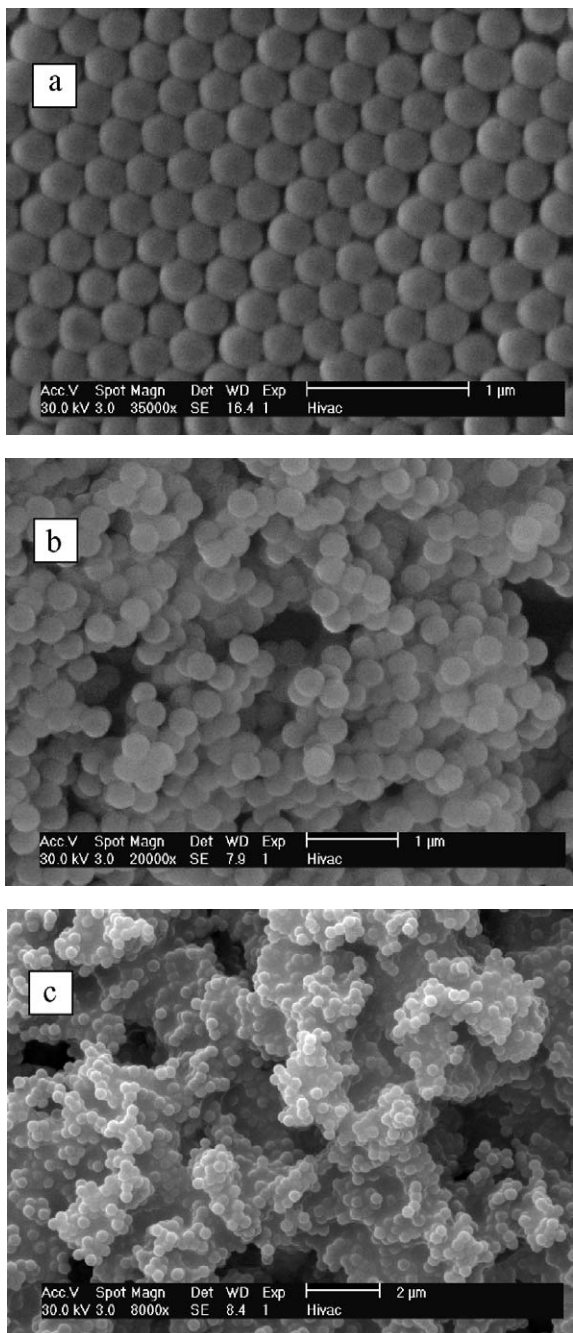


Fig. 2. Silica particle deposits on a vertical glass microslide. Particles have an average size of 244 nm. The suspensions were prepared with different solvents: (a) ethanol; (b) aqueous solution 0.15 M ionic strength; (c) aqueous solution 1.5 M ionic strength.

However, at a relatively high ionic strength (0.12 M), the open structures typical of high-ionic-strength solvents begin to show. Fig. 4 shows images of deposits of silica particles of 305 nm average diameter. Images (a) and (b) are deposits from ethanol and ultrapure water, respectively. In both cases, there is a net repulsive interaction between the particles in suspension and no aggregates have formed; for deposits obtained from ethanol, we observe that the arrangement is more

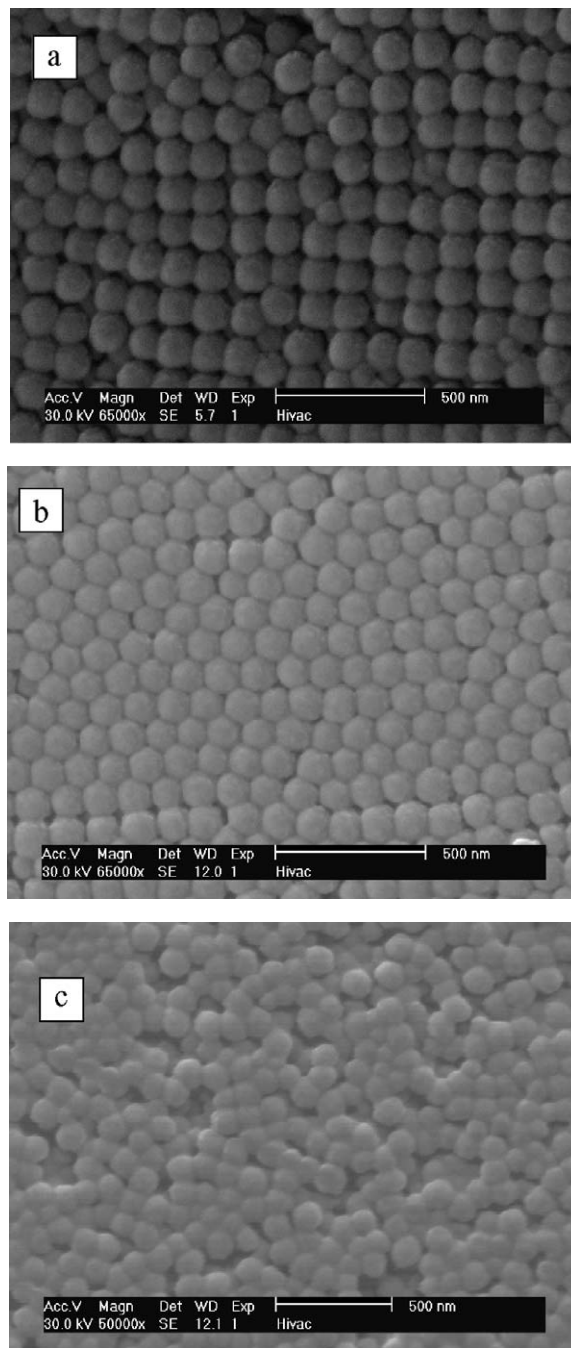


Fig. 3. Silica particle deposits on a vertical glass microslide. Particles have an average size of 88 nm. The suspensions were prepared with different solvents: (a) ultrapure water; (b) aqueous solution 0.0012 M ionic strength; (c) aqueous solution 0.12 M ionic strength.

compact. Image (c) is a deposit from high ionic strength when the open structures are formed.

Calculations of interaction energy were performed applying DLVO theory of electrostatic interactions and the set of equations derived by Kralchevsky et al. that describe capillary interactions between particles partially submerged in a liquid [11,18,19]. Figs. 5 and 6 show sample calculations for silica particles of 244 nm in diameter. Fig. 5 illustrates

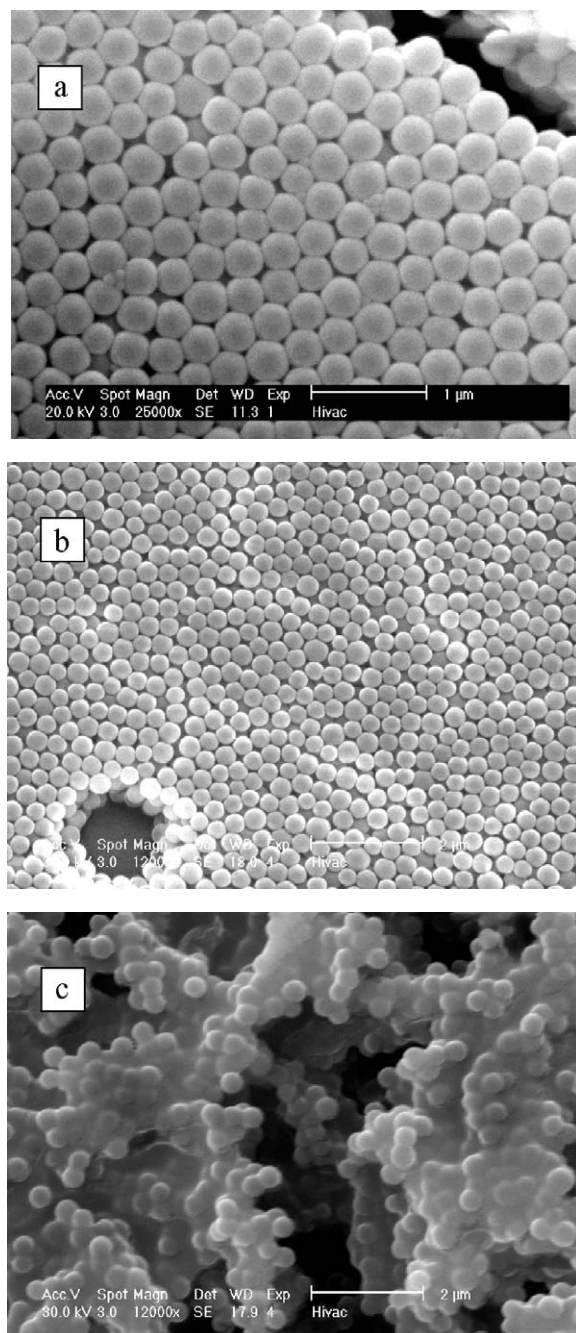


Fig. 4. Silica particle deposits on a vertical glass microslide. Particles have an average size of 305 nm. The suspensions were prepared with different solvents: (a) ethanol; (b) ultrapure water; (c) aqueous solution 0.12 M IS.

the relative importance of capillary interaction energy for the particles partially immersed in different solvents. For these calculations, we assumed a liquid level of 150 nm that corresponds to 75% of the particle diameter. The energy is (in absolute magnitude) consistently smaller for the case of the ethanol suspension than for the aqueous one. However, the results show that deposits made from ethanolic suspensions were more tightly packed. The reason for this could be the effect of the rate of evaporation of the solvent and the convective flux of particles to the substrate which in the

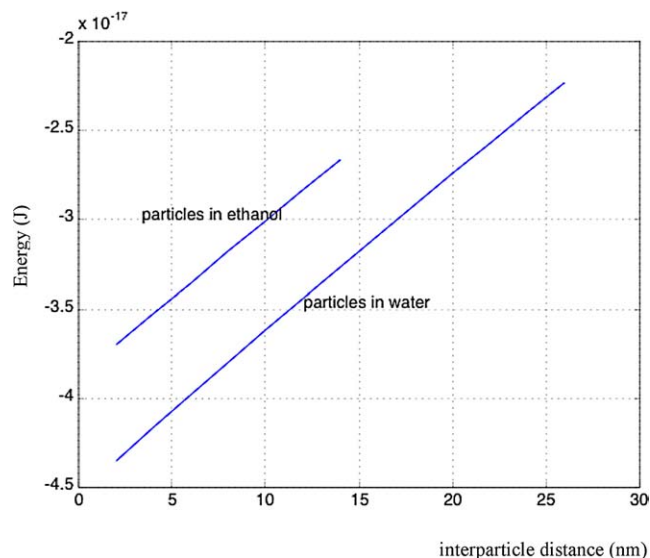


Fig. 5. Capillary interaction energy of silica particles (diameter = 244 nm) partially immersed in water and in ethanol.

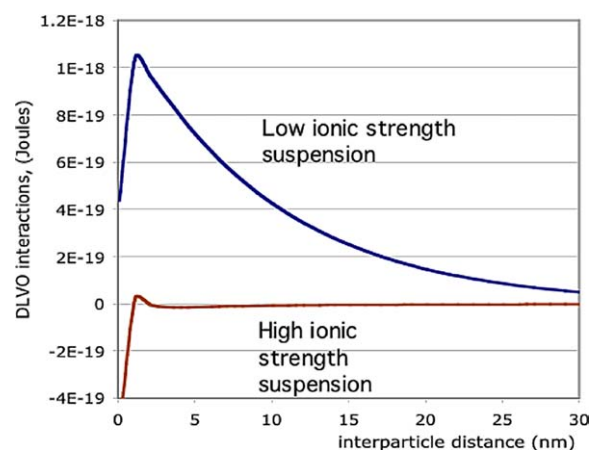


Fig. 6. DLVO interactions between silica particles (diameter = 244 nm). In the case of ultrapure water, particle–particle interactions are limited by a substantial energy barrier. At higher ionic strength, particle attachment in a secondary minimum is favored.

case of ethanol favors a more compact arrangement. Fig. 6 shows the total interaction energy (electrostatic repulsion and van der Waals attraction) for silica particles of the same size as a function of interparticle distance for the case of a low-ionic-strength suspension (0.001 M ionic strength) and a high-ionic-strength solution (0.1 M ionic strength). The data used in the calculations are: particle diameter 24 nm, Zeta potential of the particles -85 mV (low ionic strength) and -25 mV (high ionic strength), Debye reciprocal length 0.106 1/nm (low ionic strength) and 1.06 1/nm (high ionic strength), Hamaker constant $A_{131} = 7.87 \times 10^{-21}$ J. In the low ionic strength case, a high energy barrier is observed, preventing the particles from aggregate; this barrier significantly decreases in a high-ionic-strength solvent, and the energy shows a minimum at approximately 5 nm, and thus

favors the attachment and aggregation of particles, as observed in the experiments.

5. Summary and conclusions

The morphology of the particle deposits was successfully modified by varying the properties of the solvent in which the particles were suspended. Organic and low-ionic-strength solvents resulted in ordered structures of hexagonal packing. High-ionic-strength solvents yielded disorganized and open tree-like structures due to aggregation of the particles in the bulk of the suspension prior to deposition. The deposits can be used as templates for the fabrication of porous membranes; the results of this work suggest that the pore morphology of these membranes can be designed at the nanoscale by changing the surface tension and the ionic strength of the solvent from which the template is obtained.

Acknowledgments

This work was supported by the Nanoscale Science and Engineering Initiative of the National Science Foundation under NSF Award EEC-0118001.

Appendix A. Nomenclature

ΔW	interaction energy between particles
γ	surface tension of the solvent
h	meniscus elevation at the particle.
R	particle radius
α	contact angle
r	height of the protruding portion of the sphere
ψ_i	meniscus slope at the contact line (at the particle)

$\Delta\rho$	density difference (liquid–air)
g	gravity constant
l_0	thickness of the liquid layer in which the particles are partially immersed
s	1/2 distance between spheres
X_∞	value of the parameter X at infinite particle separation

References

- [1] P. Jiang, K.S. Hwang, D.M. Mittleman, J.F. Bertone, V.L. Colvin, *J. Am. Chem. Soc.* 121 (1999) 11630.
- [2] B. Gates, Y. Yin, Y. Xia, *Chem. Mater.* 11 (1999) 2827.
- [3] O.D. Velev, T.A. Jede, R.F. Lobo, A.M. Lenhoff, *Nature* 389 (1997) 477.
- [4] S.A. Johnson, P.J. Ollivier, T.E. Mallouk, *Science* 283 (1999) 963.
- [5] O.D. Velev, T.A. Jede, R.F. Lobo, A.M. Lenhoff, *Chem. Mater.* 10 (1998) 3597.
- [6] P. Jiang, J.F. Bertone, K.S. Hwang, V.L. Colvin, *Chem. Mater.* 11 (1999) 2132.
- [7] M.R. Wiesner, *J. Environ. Eng.* 125 (1999) 1124.
- [8] V. Veerapaneni, M. Wiesner, *Environ. Sci. Technol.* 31 (1997) 2738.
- [9] N.D. Denkov, O.D. Velev, P.A. Kralchevsky, I.B. Ivanov, H. Yoshimura, K. Nagayama, *Langmuir* 8 (1992) 3183.
- [10] A.S. Dimitrov, K. Nagayama, *Langmuir* 12 (1996) 1303.
- [11] P.C. Hiemenz, R. Rajagopalan, *Principles of Colloid and Surface Chemistry*, Dekker, New York, 1997.
- [12] H.C. Hamaker, *Physics* 4 (1937) 1058.
- [13] P.A. Kralchevsky, V.N. Paunov, I.B. Ivanov, K. Nagayama, *J. Colloid Interface Sci.* 151 (1992) 79.
- [14] D.Y.C. Chan, J.D. Henry, L.R. White, *J. Colloid Interface Sci.* 79 (1981) 419.
- [15] W. Stober, A. Fink, E. Bohn, *J. Colloid Interface Sci.* 26 (1968) 62.
- [16] P.K. Wiessborn, R.J. Pugh, *J. Colloid Interface Sci.* 184 (1996) 550.
- [17] V.N. Paunov, P.A. Kralchevsky, N.D. Denkov, K. Nagayama, *J. Colloid Interface Sci.* 157 (1993) 100.
- [18] P.A. Kralchevsky, K. Nagayama, *Langmuir* 10 (1994) 23.
- [19] J. Ren, S. Song, A. Lopez-Valdivieso, J. Shen, S. Lu, *J. Colloid Interface Sci.* 238 (2001) 279.